Functional recovery following traumatic spinal cord injury mediated by a unique polymer scaffold seeded with neural stem cells

Yang D. Teng*†, Erin B. Lavik†‡, Xianlu Qu*, Kook I. Park*, Jitka Ourednik*, David Zurakowski§, Robert Langer¶‖, and Evan Y. Snyder*‖****

*Departments of Neurology, Pediatrics, and Neurosurgery, Harvard Medical School, Boston, MA 02115; ‡Harvard–MIT Division of Health Sciences and Technology, and ¶Department of Chemical Engineering, Massachusetts Institute of Technology, Cambridge, MA 02139; and §Departments of Orthopaedic Surgery and Biostatistics, Children's Hospital, Boston, MA 02115

To better direct repair following spinal cord injury (SCI), we designed an implant modeled after the intact spinal cord consisting of a multicomponent polymer scaffold seeded with neural stem cells. Implantation of the scaffold–neural stem cells unit into an adult rat hemisection model of SCI promoted long-term improvement in function (persistent for 1 year in some animals) relative to a lesion-control group. At 70 days postinjury, animals implanted with scaffold-plus-cells exhibited coordinated, weight-bearing hindlimb stepping. Histology and immunocytochemical analysis suggested that this recovery might be attributable partly to a reduction in tissue loss from secondary injury processes as well as in diminished glial scarring. Tract tracing demonstrated corticospinal tract fibers passing through the injury epicenter to the caudal cord, a phenomenon not present in untreated groups. Together with evidence of enhanced local GAP-43 expression not seen in controls, these findings suggest a possible regeneration component. These results may suggest a new approach to SCI and, more broadly, may serve as a prototype for multidisciplinary strategies against complex neurological problems.

E ach year approximately 10,000 Americans sustain spinal cord injuries (SCI). Functional deficits following SCI result from damage to or severance of axons, loss of neurons and glia, and demyelination. SCI pathology is determined not only by the initial mechanical insult, but also by secondary processes including ischemia, anoxia, free-radical formation, and excitotoxicity that occur over hours and days following injury (1). Central nervous system (CNS) axonal regeneration appears to be impeded partly by myelin-associated inhibitors (1, 2), loss in adult neurons of an intrinsic ability to overcome inhibitory cues (3), and formation of a post-lesion scar barrier (4). However, if axons can traverse the injury site, there is evidence that they may regrow in unscarred regions (5, 6). Furthermore, preservation of even a small percentage of tissue significantly enhances functional recovery (7). Although there have been encouraging reports of deficit reduction (8–10) and axonal regrowth by blocking inhibitory molecules and antagonizing secondary injury mechanisms (11); myelin replacement by stem (12), Schwann (13), and olfactory ensheathing cells (14, 15); delivery of growth factors (16–18) and small molecules (19); and implantation of fetal tissue (19) and scaffolds (20–23), as yet there is no practical treatment for SCI.

We sought a conceptually new approach that simulated the architecture of the healthy spinal cord through an implant consisting of a polymer scaffold seeded with neural stem cells (NSCs) modeled after the gray and white matter of the intact cord (Fig. 1a). The scaffold's inner portion emulated the gray matter via a porous polymer layer designed to be seeded with NSCs (24) for cellular replacement as well as trophic support (Fig. 1 b and c).†† The outer portion emulated the white matter with long, axially oriented pores for axonal guidance and radial porosity to allow fluid transport while inhibiting ingrowth of scar

tissue (Fig. 1d). The scaffold is designed to be tailored to fit into a variety of cavities. In this study, the scaffold was tailored to fit into the cavity created by a midline lateral hemisection in the spinal cord of an adult rat. We hypothesized that this multicomponent, degradable, synthetic scaffold of specified architecture seeded with NSCs might mitigate secondary injury, impede glial scar formation, direct cell replacement, facilitate regeneration, and guide repair to create a more physiologically relevant structure.

Methods

Scaffold Fabrication. Both the inner and outer scaffolds were fabricated from a blend of 50:50 poly(lactic-co-glycolic acid) (PLGA) (75%, number average molecular weight, $M_n \approx 40,000$) and a block copolymer of poly(lactic-co-glycolic acid)-polylysine (25%, PLGA block $M_n \approx 30,000$, polylysine block $M_n \approx 2000$). The PLGA was chosen to achieve a degradation rate of about 30–60 days, and the functionalized polymer was incorporated to provide sites for possible surface modification. The inner scaffold was made using a salt-leaching process: a 5% (wt/vol) solution of the polymer blend in chloroform was cast over salt with a diameter range of 250–500 μm, and the solvent was allowed to evaporate. The salt was then leached in water. The oriented outer scaffold was fabricated using a solid–liquid phase separation technique (25) in the following way: A 5% (wt/vol) solution of the polymers was filtered and injected into silicone tubes which were lowered at a rate of 2.6×10^{-4} m/s into an ethanol/dry ice bath. Once frozen, the dioxane was sublimated using a shelf temperature-controlled freeze drier (VirTis). The scaffolds were then removed, trimmed, assembled, and stored in a vacuum desiccator until use.

Cell Maintenance and Seeding. Murine NSCs (clone C17.2) were maintained in serum-containing medium (24). Scaffolds were soaked in 70% ethanol for 24 h, rinsed three times in PBS, and seeded on an orbital shaker with 5×10^5 cells/ml at 37°C in a humidified 5% CO_2/air incubator. The medium was changed the next day, and the implants were incubated for 4 more days before implantation. For the cells-alone control, 10 μl of a 10^7 cells/ml
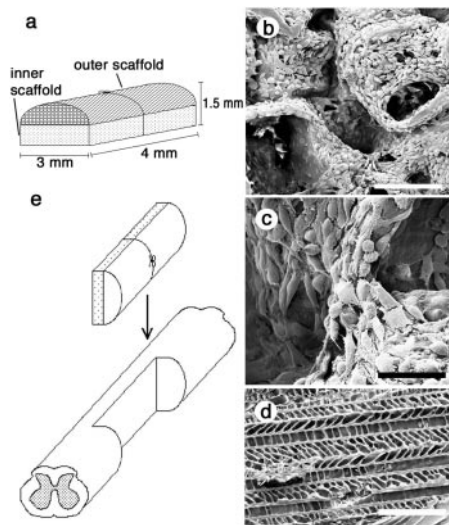
Fig. 1. (*a*) Schematic of the scaffold design showing the inner and outer scaffolds. (*b* and *c*) Inner scaffolds seeded with NSCs. (Scale bars: 200 μm and 50 μm, respectively.) The outer section of the scaffold was created by means of a solid–liquid phase separation technique that produced long, axially oriented pores for axonal guidance as well as radial pores to allow fluid transport and inhibit the ingrowth of scar tissue (*d*; scale bar, 100 μm). (*e*) Schematic of surgical insertion of the implant into the spinal cord.

suspension was injected into the cavity following the hemisection. No gelfoam or other means were used to maintain the cells in the cavity because this was thought to introduce a confounding variable.

Surgical Procedures and Animal Care. Fifty adult female Sprague–Dawley rats were used. Animals were anesthetized with a 4% chloral hydrate solution (360 mg/kg i.p.). Using a dissecting microscope, a laminectomy was made at the 9th-to-10th thoracic (T_9-T_{10}) spinal vertebrae, followed by a lateral hemisection at the T_9-T_{10} level by creating a 4-mm-long longitudinal cut along the midline of the cord with a No. 11 surgical blade, followed by lateral cuts at the rostral and caudal ends and removal of the tissue by aspiration. The surgical blade was repeatedly scraped along the ventral surface of the vertebral canal, followed by aspiration to remove any residual fibers at the lesion site. After gelfoam-triggered hemostasis occurred, an independent blinded observer confirmed the adequacy of the length and breadth of the lesion. Only at that time was the surgeon informed of the treatment (previously prepared) to be administered to the lesion. The lesion was affirmed *a priori* to be similar across all experimental groups and animals.

Either the full treatment, consisting of insertion of the NSC-seeded scaffold ("scaffold plus cells," *n* = 13; Fig. 1*e*), or one of three control treatments was performed: (*a*) polymer implant without NSCs ("scaffold alone," *n* = 11; (*b*) NSCs suspended in medium ("cells alone," *n* = 12); or (*c*) hemisection alone ("lesion control," *n* = 12).

Surgeries were performed in a randomized block design. The surgeries for the implant plus controls were performed on the same day to minimize differences between groups arising from any refinement in surgical technique during the study, and the order was varied each day to reduce surgical bias. Hemisections were alternated between the right and left sides to further reduce bias. Following either the full or control treatment, the musculature was sutured, skin closed, and the animal recovered in a clean cage on a heating pad. Ringer's lactate solution (10 ml) was given daily for 7 days post-op and bladders were evacuated twice daily until reflex bladder function was established.

Because immunosuppressive agents such as cyclosporin A have been shown to be neuroprotective on their own (26), these experiments were performed without such neuroimmunophilins to avoid this confounding variable. Donor cells were nevertheless present at the end of the study.

A separate group of scaffold plus cells animals underwent the same procedures as above and were maintained for one year.

All procedures were reviewed and approved by the Animal Care and Use Committee of Children's Hospital, Boston.

Behavioral Studies and Statistical Evaluation. One day postinjury (p.i.) and weekly thereafter, behavioral analysis was performed by two observers blinded to the treatments, using a battery of tests to rate open-field locomotion by the Basso–Beattie–Bresnahan (BBB) scale (27); the ability to maintain body position on an inclined plane; and contact righting reflex and spinal cord-mediated hindlimb withdrawal to pain (28). Behavioral tests were performed at the same time each day and graded by the same blinded observers. For the inclined plane test, the highest degree of inclination was defined as being that at which the animal could maintain its position for 5 s on two separate trials (29). Contact righting and limb withdrawal to pain were performed according to Gale *et al.* (28). One animal died following surgery because of an overdose of chloral hydrate. The remaining 49 animals survived and exhibited no signs of autophagia throughout the course of the study. One animal was excluded from the analysis because it showed incomplete paralysis at 1 day post-op. The Kolmogorov–Smirnov goodness-of-fit test was used to determine the normality (Gaussian-shaped distribution) of the data. The BBB data showed no significant departure from a normal distribution for all time points beyond day 1, so parametric methods were used including repeated-measures analysis of variance (ANOVA) and Bonferroni *post hoc* analysis for multiple group comparisons to determine the statistical significance of the results. The inclined plane data showed a significant departure from a normal distribution and was analyzed with the Kruskal–Wallis H-test, followed by the Mann–Whitney *U* test to identify specific group differences when the Kruskal–Wallis test showed significance ($P < 0.05$).

Tissue Processing for Histology. Following perfusion, spinal cords were carefully dissected, postfixed overnight in 4% paraformaldehyde, dehydrated overnight at 4°C in 30% sucrose, and frozen in isopentane. Two centimeter blocks of the thoracic region of the cords including injury epicenters were embedded in OCT and cryosectioned. Longitudinal sections for hematoxylin/eosin (H&E) were obtained from a depth of 1.6 mm into the cord (from the dorsal side). Neurofilament sections were 80 μm dorsal to H&E sections.

BDA Tracing. BDA (biotinylated dextran amine; Molecular Probes, 10% wt/vol solution) was injected at ten points in the sensory motor cortex contralateral to the side of the spinal cord hemisection at or beyond 70 days p.i. (30). Animals were maintained for 4 more weeks then killed. Following cryosectioning of the tissue, BDA was revealed histochemically on mounted sections by using a Vector Elite ABC kit (Vector Laboratories) followed by development with DAB and light counterstaining with neutral red.

Immunocytochemistry. Immunocytochemistry was performed on 20-μm mounted sections employing the following antibodies: anti-neurofilament 200 (NF) (Sigma; 1:200); anti-glial fibrillary acidic protein (GFAP; Sigma; 1:80); M2 (a mouse-specific marker; gift from Carl Lagenaur, University of Pittsburgh; 1:5); anti-GAP-43 (gift from Larry Benowitz, Children's Hospital, Boston; 1:50,000). Briefly, sections were incubated with primary antibody for 1 h at 37°C followed by the appropriate secondary antibody for 1 h at 37°C. Blocking solution consisted of 3%
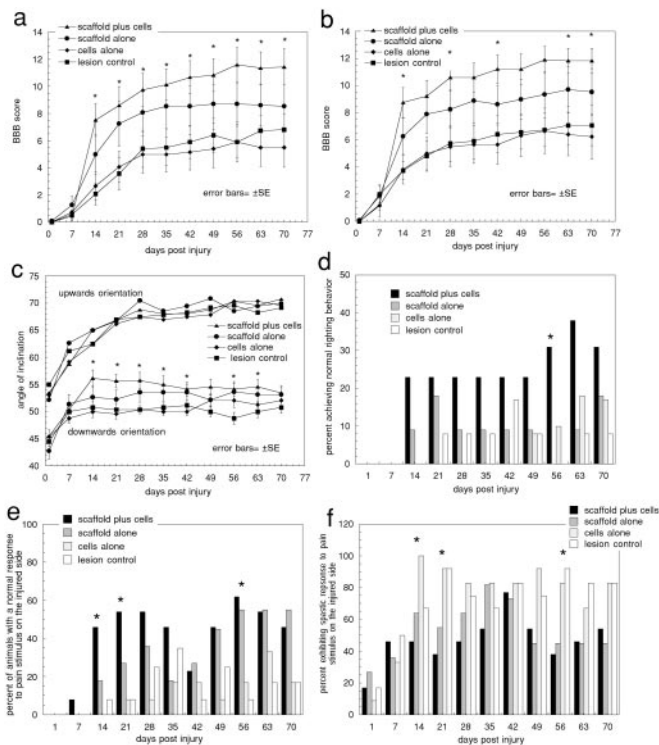
Fig. 2. (a) BBB open-field walking scores for the four groups on the ipsilateral, lesioned side. Hindlimbs were assessed independently to determine the degree of asymmetry. The *rate* of improvement for the scaffold plus cells group was significantly greater than the rate for the cells-alone ($P < 0.001$) and lesion-control groups ($P = 0.004$; two-way repeated measures of ANOVA). For absolute score attained, the scaffold plus cells group showed significant improvement in open-field locomotion compared with the cells-alone ($P = 0.006$) and lesion-control groups ($P = 0.007$) for all time points from 14 days p.i. on (ANOVA, Bonferroni *post hoc* analysis). (b) BBB open-field walking scores for the contralateral unlesioned hindlimb. There is only a 1–2 point difference between the lesioned (see *a*) and unlesioned sides, indicating that the walking behavior of the groups was relatively symmetric overall and that both sides were impacted by this unilateral lesion. Individual animals did, however, exhibit a degree of asymmetry in their stepping with a twisted trunk position leading to the rotation of both hindlimbs to one side of their bodies. (*c*) Inclined plane results. When facing upwards, animals in the four groups are statistically similar for all time points (Kruskal–Wallis test) indicating that they were generally similar in strength. When facing downwards, the scaffold plus cells group performance showed statistically significant improvement on all days from day 14 on (except days 49 and 70) compared with the cells-alone and lesion-control groups (Kruskal–Wallis test). Although the data showed significant departure from the Gaussian distribution, parametric analysis revealed similar results to nonparametric analysis, and the results are represented in the figure by their means for visual clarity. (*d*) Righting reflex results. The scaffold plus cells group exhibited a significantly higher percentage of normal righting on day 56 as compared with the lesion-control (Pearson χ^2 test of independence). (*e*) Percent of animals with a normal pain reflex in response to toe pinching was significantly higher in the plus cells group on the days marked by the asterisks (Pearson χ^2 test). (*f*) Percent of animals exhibiting a spastic response to the same toe pinching stimuli.

serum in which the secondary antibody was raised and 5% BSA (Vector Laboratories).

Results and Discussion

Fig. 2 *a* and *b* shows the mean BBB open-field walking scores (27) for the four experimental groups on their ipsilateral, "lesioned" (Fig. 2*a*), and contralateral, "unlesioned" (Fig. 2*b*) sides. The open-field locomotion of representative animals from the scaffold plus cells and lesion-control groups who performed near the mean of their groups at day 70 is shown in Movie 1,
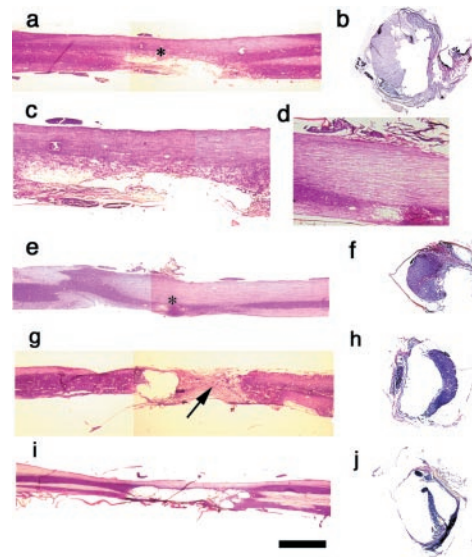

Fig. 3. Hematoxylin/eosin (H&E) staining of representative 20-μm-thick longitudinal and transverse sections from each group. (*a* and *b*) Scaffold plus cells sections in longitudinal and cross section, respectively. Area with an asterisk in *a* is shown at higher power in *c*. (*a*) A section from the cord of the scaffold plus cells animal from Movie 1, which is published as supporting information. Although there is some degeneration of gray matter, there is preserved tissue near the injury epicenter as well as rostral and caudal to the injury. There is only limited scar tissue at the injury epicenter on the lesioned side (*c*). (*d*–*f*) Scaffold-alone sections. Area with an asterisk in *e* is shown at higher power in *d*. (*g* and *h*) Cells-alone sections. Note the degradation of tissue both rostral and caudal to the injury epicenter as well as the extent of scar tissue at the injury epicenter on both the lesioned and unlesioned sides (arrow). (*i* and *j*) Lesion-control sections. In *i* there is a small degree of white matter on the unlesioned side, but the lesioned region has expanded almost 2-fold from the original lesion size, a 4-mm lateral hemisection. In *j* there is an incomplete rim of peripheral white matter on the unlesioned side. (Scale bar, 2.5 mm.)

which is published as supporting information on the PNAS web site, www.pnas.org. Open-field locomotion on both the ipsilateral and contralateral sides in the scaffold plus cells group was significantly enhanced in the subchronic phase (up to 28 days p.i.) with respect to both *rate* and *absolute level* of improvement achieved; this enhanced performance was maintained into the chronic phase of recovery (70 days p.i.). Performance of the unlesioned side mirrored the lesioned side both in absolute mean values achieved and statistical significance. Impairment of the contralateral side likely reflects the severity of the hemisection (see surgical procedures for details) in which 4 mm of tissue was removed, leading to severance of a number of blood vessels that may have resulted in ischemia- and hypoxia-related secondary injury on the unlesioned side. Similar phenomena have been reported (31). Both hindlimbs were affected, and recovery of both was improved by the scaffold plus cells intervention. The scaffold plus cells group, in the late chronic stage (i.e., 56 days p.i. and later), achieved a stabilized mean BBB score of approximately 12, which corresponds to frequent-to-consistent weight-supported plantar-stepping and occasional forelimb-hindlimb coordination. In contrast, the cells-alone and lesion-control groups only achieved stabilized mean BBB scores of ≈6 and 7, respectively. Encouragingly, the scaffold-alone group also achieved a mean BBB score of ≈9, which indicates the onset of weight-supported locomotion, suggesting that even the scaffold alone is capable of leading to improvement in functional recovery. Defining the onset of significant walking behavior as achieving a BBB score of 10 or greater at 70 days p.i., 69% of the
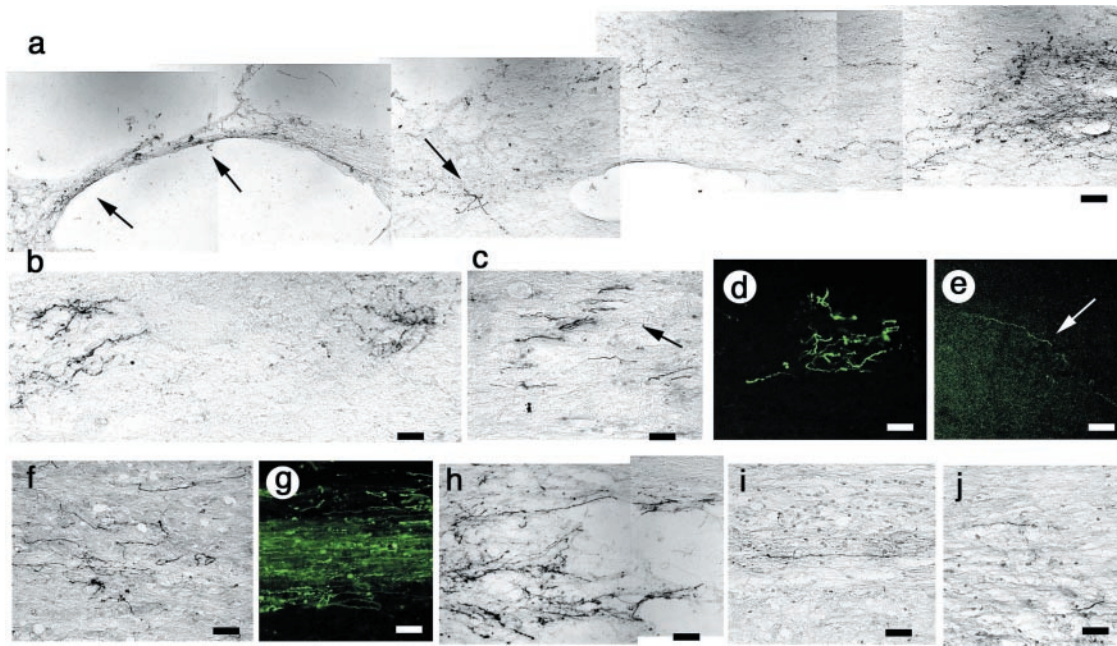
Fig. 4. (a) BDA tracing of the corticospinal tract in a scaffold-alone animal. BDA was injected into the sensorimotor cortex contralateral to the spinal cord injury at or beyond 70 days p.i. such that BDA-positive fibers would be visible at the site of, or caudal to, the spinal cord lesion if corticospinal tract fibers were present and passing through the injury site. Arrows indicate where the tracer passes into the lesioned side of the cord. Note the tortuous path of the fibers (arrows; see text). The rostral end is to the right, and the lesion cavity is on the bottom. (b) Positive BDA tracing caudal to the injury in the same cord as in a. (c) GAP-43, a marker for regenerating axons, is positive in the same cord as seen in a and b just rostral to the injury. Likewise, scaffold plus cells cords exhibit BDA tracing with the same tortuousity immediately (d) rostral to as well as (e) caudal to the injury, and (f) a large number of GAP-43-positive axons just rostral to the injury. The cells-alone (g) and lesion-control cords (h) exhibit BDA staining rostral to the injury but not caudal, and there are minimal fibers positive for GAP-43 (i, cells alone; j, lesion control; scale bars in a–b, d–e, and g–h, 10 μm; in c, f, and i–j, 20 μm).

scaffold plus cells groups, 54% of the scaffold alone, but only 17% of the cells-alone and 33% of lesion-control groups attained BBB score of at least 10.

For inclined plane performance, animals were tested facing both upwards and downwards (Fig. 2c). Whereas performance in the upward-facing orientation reflects forelimb strength, which should be unaffected by this injury in healthy animals, performance facing downwards measures coordinated hindlimb motor function (28). In the upwards orientation, all groups exhibited statistically similar performances, suggesting that the animals had similar forelimb strength. However, the scaffold plus cells group showed statistically significant improvement with respect to the cells-alone and lesion-control groups in the downward-facing orientation on all days beyond day 7 (except days 49 and 70). Overall, the inclined plane results mirror the BBB scoring, suggesting that the scaffold plus cells intervention is associated with significant long-term improvement of motor function.

Spinal cord mediated reflexes also showed a trend toward improvement following the scaffold plus cells intervention as compared with cells alone and lesion controls. In particular, a higher percentage of animals in the scaffold plus cells group exhibited normal righting behavior on all days beyond day 14 (Fig. 2d).

The scaffold plus cells group demonstrated more normal sensory responses. Fig. 2e shows the percentage of animals after SCI in each group with a normal pain withdrawal reflex induced by a controlled brief pinch of the toes (28). At 70 days p.i., approximately 50% of the animals regained a normal pain withdrawal reflex (scored as a 2 and representing an immediate and controlled withdrawal reflex in response to the stimuli) on the lesioned side in the groups treated with scaffolds plus cells and scaffold alone (Fig. 2e). In contrast, only approximately 15% of the cells-alone and lesion-control groups regained a normal pain withdrawal reflex on the lesioned side. Fig. 2f shows the

percentage of animals with a spastic pain withdrawal reflex, which is defined as an immediate but hyperactive response in which the limb demonstrates spasms upon stimulation. Overall, the scaffold plus cells and scaffold-alone interventions appear to lead to a more favorable outcome of the normal, nonspastic response, suggesting more normal spinal cord-mediated reflexes.

Histology, tract tracing, and immunocytochemistry were performed on all cords to help elucidate possible mechanisms leading to the observed functional recovery. The images of the lesion area presented in Fig. 3 are representative of each experimental group at 120 days p.i., and were obtained from animals whose BBB scores placed them near the mean of their respective groups. The sections are all from the same depth at 1.6 mm into the cord. The cross sections were obtained through the injury epicenter, which was determined by the least amount of contralateral tissue sparing in each cord. The scaffold plus cells (Fig. 3 a–c) and scaffold-alone cords (Fig. 3 d–f) at 120 days p.i. had very limited residual lesions that barely crossed the midline of the cord (Fig. 3 a and c). In some cases, there appeared to be newly formed tissue within the injury epicenter (Fig. 3 d and e). The cells-alone (Figs. 3 g and h) and lesion-control cords (Fig. 3 i and j) demonstrated marked residual lesions 5–6 mm in length and encompassing the majority of the width of the cord. Furthermore, both the lesion-control and cells-alone cords exhibited atrophy both rostral and caudal to the injury. In some of the cells-alone and lesion-control cords, scar tissue and cysts were seen. Fig. 3g, a longitudinal section of a typical cells-alone cord, demonstrates the epidural scar tissue (marked by the arrow) as well as the cyst formation seen in some of the cells-alone and lesion-control cords, but not seen in the scaffold plus cells or scaffold alone cords.

It is hypothesized that the scaffold may impede scarring and subsequent cyst formation. The mechanism for this is not yet

known but may be correlated with inhibition of cellular ingrowth by the outer scaffold. *In vitro*, the outer scaffold appears to inhibit the ingrowth of a variety of cell types, including fibroblasts, into the porous scaffold for at least 2 weeks (data not shown). The absence of scar formation is correlated with a higher degree of tissue preservation at the injury epicenter as well as preservation of tissue rostral and caudal to the epicenter. The absence of scar tissue may account for the diminished atrophy in the spinal cords of the scaffold-containing groups as compared with the cells alone and lesion controls. The expansion of the lesion has been correlated with secondary injury processes (1), and the size of the lesion appears to correlate with the degree of functional deficit (32).

Although tissue preservation appears to be the primary factor accounting for the improved functional recovery in the scaffold plus cells group, it may be augmented by possible regenerative processes. BDA tracing of the corticospinal tract (30), coupled with immunocytochemistry for GAP-43, a protein up-regulated in the growth cones of regenerating axons (33), suggests that there may be a component of regeneration occurring. Fig. 4 *a* and *b* shows BDA tracing of the corticospinal tract on the lesioned side of the cord in the scaffold-alone group. There is positive tracing of fibers through the injury epicenter (Fig. 4*a*, arrows) and caudal to the injury (Fig. 4*b*). For BDA-positive corticospinal tract axons to be detectable in regions caudal to the injury epicenter, BDA, injected in the motor cortex, had to have been transported in an antegrade manner along either spared or regenerated corticospinal fibers. The tortuous path of the traced fibers as well as the multipolar nature of the portions caudal to the injury site is most consistent with morphological profiles generally seen in regenerating axons as opposed to spared fibers, which would retain their straight, nontortuous profile. There are a large number of GAP-43-positive fibers just rostral to the injury site in this cord (Fig. 4*c*, arrows), further suggesting a possible component of regeneration at day 70 p.i. Likewise, in the scaffold plus cells cords, there was BDA-positive tracing both rostral and caudal to the injury epicenter as well as GAP-43 immunopositive staining just rostral to the injury (Fig. 4 *d*–*f*). In contrast, the cells-alone and lesion-control cords showed positive BDA tracing rostral but not caudal to the injury epicenter (Fig. 4 *g* and h), and very few GAP-43-positive fibers (Fig. 4 *i* and *j*). BDA tracing plus GAP-43 immunostaining, though frequently used indicators of regeneration (27), are not definitive markers.

Both the scaffold plus cells and scaffold-alone cords exhibited immunopositive staining for an antibody against neurofilament (NF) within the injury epicenter (Fig. 5 *a* and *b*). In Fig. 5*b*, the region of immunopositive staining is within the space of the primary injury, suggesting that the newly formed tissue contains neurons or neuronal elements. Fig. 5*c* shows immunohistology of a scaffold plus cells cord just rostral to the injury epicenter employing an NF-antibody (green) plus mouse-specific antibody, M2 (red), to identify donor murine NSC-derived cells within the rat host. Donor-derived cells were identified in both cells-alone and scaffold plus cells cords rostral to the injury epicenter (Fig. 5*c*, red immunostaining). Confocal microscopy of the expression pattern of these markers, however, suggests that the donor cells were not immunopositive for NF, suggesting that the neurons were actually of host origin. In comparison to the scaffold-containing groups, the lesion-control cords showed much less immunopositive staining for NF throughout the thoracic region of the cord (Fig. 5*d*). Although the donor NSCs do not appear to be immunopositive for NF, they are also not largely immunopositive for GFAP (Fig. 5*e*), suggesting that they are not contributing to the glial scar. The majority of the donor cells are, in fact, immunopositive for nestin (Fig. 5*f*), suggesting that they remained largely undifferentiated. It is possible that the major contribution of the NSCs was trophic support rather than cellular
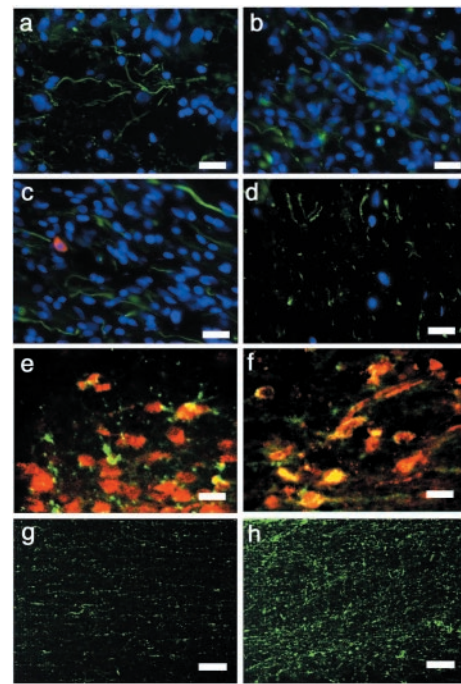

Fig. 5. All longitudinal sections. (*a*) A scaffold plus cells section at the injury epicenter immunostained for NF (green) and counterstained with DAPI (blue). (*b*) Scaffold-alone section at the injury epicenter exhibiting NF immunoreactivity (green) within the region excised by the initial lesion, suggesting that the new tissue contains neurons or neuronal elements (blue, DAPI). (*c*) Double immunostaining for NF (green) and the mouse-specific antigen M2 used to identify donor cells (red) in a scaffold plus cells cord and DAPI (blue). The cord has extensive NF immunopositivity, but there is no clear colocalization of NF and M2, suggesting that the NF+ cells were of host-origin. (*d*) There are few NF+ cells near the injury epicenter in the lesion-control cord. (*e*) Scaffold plus cells section doubled-immunostained for GFAP (green) and M2 (red). The majority of donor-derived cells (red) are not double-labeled for GFAP, suggesting that they do not contribute to the astroglial scar. (*f*) Most donor cells (stained with the M2 antibody, green in this figure) are double-labeled for nestin (red in this figure), as seen by confocal microscopy. GFAP immunostaining (green) in the spared tissue contralateral to the hemisection in a scaffold plus cells cord (*g*) compared with a lesion-control cord (*h*). There is a far greater incidence of astrocytes at the injury epicenter of the lesion-control compared with the scaffold-alone cord. (Scale bars: *a*–*f*, 20 μm; *g*–*h*, 10 μm.)

replacement.[††] Although there were substantially fewer donor-derived cells in the cords receiving NSCs alone, the NSCs appear to have behaved in a similar way, remaining largely nestin-positive.

The functional results suggest that the scaffold played an important role in recovery. Immunostaining for GFAP in the scaffold-alone and lesion controls (Fig. 5 *h* and *g*) exhibited a smaller population of astrocytes in the injury epicenter of the former than of the latter. The lesion-control and cells-alone cords, in general, exhibited larger populations of GFAP-positive astrocytes at their lesion epicenters than the scaffold plus cells and scaffold alone cords. Although controversial, astrocytes have been correlated with formation of the inhibitory glial scar. Thus, a reduction in astrocyte ingrowth following injury is believed to be desirable. Although the mechanism by which the scaffold may augment recovery is not known, *in vitro* evidence, as noted above, suggests that the outer scaffold inhibits ingrowth of a variety of cell types. Because the scaffold is completely degradable, this inhibition is temporary. However, the outer scaffold may reduce inflammatory cell infiltration that occurs shortly after SCI, in turn reducing astrogliosis (34).

The mechanisms by which the scaffold and NSCs augment functional recovery need to be explored further. A detailed

anatomical study at multiple time points correlated with the current behavioral results (including quantitative analysis of cell types involved and the number of myelinated and unmyelinated axons) may help to elucidate some mechanisms. In addition, because the corticospinal tract in the rat is not mainly involved in locomotor function, regenerative activity in more relevant but less accessible tracts (e.g., rubrospinal tracts) needs to be examined in future studies. Electrophysiology may allow a better understanding of the nature of the neuroprotected tissue along with any regenerated neural tissue at the injury site. The use of additional animal models may also be helpful.

In summary, implantation of the scaffold with NSCs significantly improves functional recovery as compared with cells alone and lesion controls. Indeed, scaffold plus cell animals maintained for 1 year p.i. continue to show enduring recovery with respect to BBB scoring ($n = 8$). Although the scaffold alone appears to play a significant role in functional recovery following hemisection by reducing epidural and glial scar formation, the combination of the NSCs and scaffold is critical for the greatest recovery.

Satisfactory outcomes have not been achieved to date in treating SCI by means of a single approach. Our results suggest that, with further study, the concept of polymer scaffolds seeded with NSCs may contribute to a new multifaceted approach for the treatment of SCI. More broadly, this work may provide a prototype for other multidisciplinary strategies for addressing complex neurological maladies.

1. Beattie, M. S., Farooqui, A. A. & Bresnahan, J. C. (2000) *J. Neurotrauma* **17,** 915–925.
2. Chen, M. S., Huber, A. B., Haar, M. E. v. d., Frank, M., Schnell, L., Spillmann, A. A., Christ, F. & Schwab, M. E. (2000) *Nature (London)* **403,** 434–439.
3. Cai, D., Qui, J., Cao, Z., McAtee, M. & Bregman, B. S. (2001) *J. Neurosci.* **21,** 4731–4739.
4. Fitch, M. T., Doller, C., Combs, C. K., Landreth, G. E. & Silver, J. (1999) *J. Neurosci.* **19,** 8182–8198.
5. Davies, S. J., Fitch, M. T., Memberg, S. P., Hall, A. K., Raisman, G. & Silver, J. (1997) *Nature (London)* **390,** 680–683.
6. Neumann, S. & Woolf, C. (1999) *Neuron* **23,** 83–91.
7. Blight, A. R. (1983) *Neuroscience* **10,** 521–543.
8. Cheng, H., Cao, Y. & Olson, L. (1996) *Science* **273,** 510–513.
9. McDonald, J. W., Liu, X.-Z., Qu, Y., Liu, S., Mickey, S. K., Turetsky, D., Gottleib, D. I. & Choi, D. W. (1999) *Nat. Med.* **5,** 1410–1412.
10. Imaizumi, T., Lankford, K. L., Burton, W. V., Fodor, W. L. & Kocsis, J. D. (2000) *Nat. Biotechnol.* **18,** 949–953.
11. Bregman, B. S., Kunkel-Bagden, E., Schnell, L., Dai, H. N., Gao, D. & Schwab, M. E. (1995) *Nature (London)* **378,** 498–501.
12. Liu, S., Qu, Y., Stewart, T. J., Howard, M. J., Chakrabortty, S., Holekamp, T. F. & McDonald, J. W. (2000) *Proc. Natl. Acad. Sci. USA* **97,** 6126–6131.
13. Xu, X., Zhang, S.-X., Li, H., Aebischer, P. & Bunge, M. (1999) *Eur. J. Neurosci.* **11,** 1723–1740.
14. Ramón-Cueto, A., Cordero, M. I., Santos-Benito, F. F. & Avila, J. (2000) *Neuron* **25,** 425–435.
15. Li, Y., Field, P. M. & Raisman, G. (1997) *Science* **277,** 2000–2002.
16. Teng, Y. D., Mocchetti, I., Taveira-DaSilva, A. M., Gillis, R. A. & Wrathall, J. R. (1999) *J. Neurosci.* **19,** 7037–7047.
17. Xu, X. M., Guénard, V., Kleitman, N., Aebischer, P. & Bunge, M. B. (1995) *Exp. Neurol.* **134,** 261–272.
18. Grill, R., Murai, K., Blesch, A., Gage, F. H. & Tuszynski, M. H. (1997) *J. Neurosci.* **17,** 5560–5572.
19. Diener, P. S. & Bregman, B. S. (1998) *J. Neurosci.* **18,** 763–778.
20. Vacanti, M., Leonard, J., Dore, B., Bonassar, L., Cao, Y., Stacheleck, S., Vacanti, J., O'Connell, F., Yu, C., Farwell, A. & Vacanti, C. (2001) *Transplant. Proc.* **33,** 592–598.
21. Woerly, S., Petrov, P., Sykova, E., Roitbak, T., Simonova, Z. & Harvey, A. (1999) *Tissue Eng.* **5,** 467–488.
22. Gautier, S. E., Oudega, M., Fragoso, M., Chapon, P., Plant, G. W., Bunge, M. B. & Parel, J.-M. (1998) *J. Biomed. Mater. Res.* **42,** 642–654.
23. Holmes, T., Lacalle, S. d., Su, X., Liu, G., Rich, A. & Zhang, S. (2000) *Proc. Natl. Acad. Sci. USA* **97,** 6728–6733.
24. Yandava, B., Billinghurst, L. & Snyder, E. (1999) *Proc. Natl. Acad. Sci. USA* **96,** 7029–7034.
25. Schurgens, C., Maquet, V., Grandfils, C., Jerome, R. & Teyssie, P. (1996) *Polymer* **37,** 1027–1038.
26. Guo, X., Dillman, J., Dawson, V. & Dawson, T. (2001) *Ann. Neurol.* **50,** 6–16.
27. Basso, D. M., Beattie, M. S. & Bresnahan, J. C. (1995) *J. Neurotrauma* **12,** 1–21.
28. Gale, K., Kerasidis, H. & Wrathall, J. (1985) *Exp. Neurol.* **88,** 123–134.
29. Rivlin, A. & Tator, C. (1977) *J. Neurosurg.* **47,** 577–581.
30. Weidner, N., Grill, R. J. & Tuszynski, M. H. (1999) *Exp. Neurol.* **160,** 40–50.
31. Dusart, I. & Schwab, M. (1994) *Eur. J. Neurosci.* **6,** 712–714.
32. Noble, L. J. & Wrathall, J. R. (1989) *Exp. Neurol.* **103,** 34–40.
33. Benowitz, L. I., Apostolides, P. J., Perrone-Bizzozero, N., Finklestein, S. P. & Zwiers, H. (1988) *J. Neurosci.* **8,** 339–352.
34. Fitch, M. T. & Silver, J. (1997) *Exp. Neurol.* **148,** 587–603.

MEDICAL SCIENCES